Astronomy & Astrophysics manuscript no. spec8˙fin
July 9, 2012

© ESO 2012

arXiv:1207.1530v1 [astro-ph.CO] 6 Jul 2012

Cl 1103.7−1245 at $z = 0.96$: the highest redshift galaxy cluster in the EDisCS survey[⋆]

Benedetta Vulcani[1,2⋆⋆], Alfonso Aragón-Salamanca[3], Bianca M. Poggianti[2], Bo Milvang-Jensen[4], Anja von der Linden[5], Jacopo Fritz[6], Pascale Jablonka[7,8], Olivia Johnson[9], and Dennis Zaritsky[10]

[1] Astronomical Department, Padova University, vicolo dell'Osservatorio 3, I-35122 Padova, Italy
[2] INAF-Astronomical Observatory of Padova, Vicolo dell'Osservatorio 5, I - 35122 Padova, Italy
[3] School of Physics and Astronomy, University of Nottingham, Nottingham NG7 2RD, UK
[4] Dark Cosmology Centre, Niels Bohr Institute, University of Copenhagen, Juliane Maries Vej 30, 2100 Copenhagen, Denmark
[5] Kavli Institute for Particle Astrophysics and Cosmology, Stanford University, Stanford, CA 94309, USA
[6] Sterrenkundig Observatorium Vakgroep Fysica en Sterrenkunde Universeit Gent, Krijgslaan 281, S9 9000 Gent, Belgium
[7] Observatoire de Genéve, Laboratoire d'Astrophysique Ecole Polytechnique Federale de Lausanne (EPFL), 1290 Sauverny, Switzerland
[8] GEPI, Observatoire de Paris, CNRS UMR 8111, Université Paris Diderot, 92125 Meudon Cedex, France
[9] Royal Observatory, Blackheath Avenue Greenwich, SE10 8XJ, UK
[10] Steward Observatory, University of Arizona, 933 North Cherry Avenue, Tucson, AZ 85721, USA

Accepted .... Received ..; in original form ...

ABSTRACT

We present new spectroscopic observations in a field containing the highest redshift cluster of the ESO Distant Cluster Survey (EDisCS). We measure galaxy redshifts and determine the velocity dispersions of the galaxy structures located in this field. Together with the main cluster Cl 1103.7−1245 ($z = 0.9580$; $\sigma_{\rm clus} = 522 \pm 111\,{\rm km\,s^{-1}}$) we find a secondary structure at $z = 0.9830$, Cl 1103.7−1245c. We then characterize the galaxy properties in both systems, and find that they contain very different galaxy populations. The cluster Cl 1103.7−1245 hosts a mixture of passive elliptical galaxies and star-forming spirals and irregulars. In the secondary structure Cl 1103.7−1245c all galaxies are lower-mass star-forming irregulars and peculiars. In addition, we compare the galaxy populations in the Cl 1103.7−1245 $z = 0.9580$ cluster with those in lower redshift EDisCS clusters with similar velocity dispersions. We find that the properties of the galaxies in Cl 1103.7−1245 follow the evolutionary trends found at lower redshifts: the number of cluster members increases with time in line with the expected growth in cluster mass, and the fraction of passive early-type galaxies increases with time while star-forming late types become less dominant. Finally, we find that the mean stellar masses are similar in all clusters, suggesting that massive cluster galaxies were already present at $z \sim 1$.

Key words. galaxies: clusters: general – galaxies: distances and redshifts – galaxies: evolution

1. Introduction

Clusters of galaxies, the largest gravitationally-bound systems evolving from large-scale fluctuations, provide important constraints on cosmological models and are also useful laboratories to study the effect of environment on galaxy evolution. In order to place the strongest constraints on cosmological parameters and explore a broad look-back-time baseline for evolutionary studies, clusters at redshifts as high as z~1 are crucial (e.g., Aragon-Salamanca et al. 1993; Levine et al. 2002; Lima & Hu 2004).

Unfortunately, spectroscopic surveys of sizeable galaxy samples in very distant clusters ($z \sim 1$) are quite rare. At lower redshifts ($z \sim 0.2 - 0.8$), 68 clusters have been studied todate, including the spectroscopic surveys of Couch & Sharples (1987), and the work of the CNOC and MORPHs collaborations (Yee et al. 1996; Balogh et al. 1997; Dressler et al. 1999; Poggianti et al. 1999) and, more recently, the EDisCS (White et al. 2005) and ICBS (Oemler et al. in preparation) projects. In addition small samples and individual clusters have also been studied (e.g. van Dokkum et al. 2000; Tran et al. 2003; Kelson et al. 1997, 2006; Bamford et al. 2005; Serote Roos et al. 2005; Moran et al. 2005).

At even higher redshifts, 47 clusters have been studied (Postman et al. 1998, 2001; Olsen et al. 2005; Gilbank et al. 2007; Muzzin et al. 2012), complemented with the analysis of individual rich clusters (e.g. van Dokkum et al. 2000; Jørgensen et al. 2005, 2006; Tanaka et al. 2006; Demarco et al. 2007; Tran et al. 2007; Fassbender et al. 2011). However, detailed spectroscopic studies of clusters at $z \sim 1$ are still relatively few and a clear picture of the galaxy population at this cosmic time has not emerged yet.

For distant cluster studies, the ESO Distant Cluster Survey (EDisCS, White et al. 2005) represents an important step toward the understanding of the star formation histories of cluster galaxies. It targeted 20 galaxy clusters, drawn from the Las Campanas Distant Cluster Survey (LCDCS) catalog (Gonzalez et al. 2001), with redshifts between 0.4 and 0.8. For these clusters a vast, high-quality, homogeneous multi-wavelength dataset has been assembled, making EDisCS arguably the best-studied cluster sample at these redshifts.

[⋆] Based on observations collected at the European Southern Observatory (ESO) Chile, as part of programme 080.A-0180(A), as well as on programme 166.A-0.162 (the ESO Distant Cluster Survey).

[⋆⋆] benedetta.vulcani@oapd.inaf.it

Deep spectroscopy with FORS2/VLT was initially obtained for 18 of the fields (Halliday et al. 2004; Milvang-Jensen et al. 2008). Spectroscopic targets were selected with the aim of producing an unbiased sample of cluster galaxies. During the observation of the LCDCS field at $z = 0.83$ (Gonzalez et al. 2001), a distant cluster at the LCDCS position but at a substantially higher redshift ($z = 0.96$) than that inferred from the confirmation spectroscopy was discovered (for details, see White et al. 2005). As spectroscopic targets were pre-selected using photometric redshifts to minimize field contamination, the EDisCS spectroscopic sample in this field was biased against $z = 0.96$ galaxies. The discovery of nine galaxies at this redshift revealed the presence of a moderately rich cluster, with a preliminary spectroscopic velocity dispersion of $\sigma^{\rm spec}_{\rm clus} = 600^{+100}_{-150}\,{\rm km\,s^{-1}}$. Given the large number of cluster members found in observations biased against them, it seemed likely that the structure was richer still.

The richness of Cl 1103.7−1245 was confirmed by its clear detection in the weak lensing analysis of Clowe et al. (2006). This study indicates a mass concentration corresponding to a cluster with a velocity dispersion $\sigma^{\rm lensing}_{\rm clus} = 899^{+129}_{-159}\,{\rm km\,s^{-1}}$ centred on the brightest cluster galaxy with $z = 0.96$. As noted in that paper, however, the lensing analysis might have overestimated the cluster mass due to the effect of mass belonging to two secondary structures at $z = 0.63$ and $z = 0.70$.

Soft diffuse X-ray emission from hot ICM in Cl 1103.7-1245 was also clearly detected in deep 90ks XMM-Newton observations (Johnson et al., in preparation). The X-ray detection was coincident with both the Brightest Cluster Galaxy (BCG) and the weak-lensing detection and was of sufficient statistical quality that the X-ray luminosity ($L_X = 3.9^{+0.5}_{-1.0} \times 10^{43}\,{\rm erg\,s^{-1}}$) and temperature ($T = 3.2^{+1.3}_{-0.8}\,{\rm keV}$) can be independently constrained by the X-ray spectrum (Johnson et al., in preparation). Cl 1103.7−1245 is among the coolest and least luminous $z \sim 1$ clusters to have been detected in X-rays.

Additional spectroscopy for this cluster was obtained using FORS2 at the VLT, significantly expanding the redshift range of the EDisCS cluster sample. In this paper we present these new spectroscopic observations, the data reduction, and a detailed analysis of the galaxies in the field of Cl 1103.7−1245. In addition we compare this cluster's galaxy properties with those of the galaxy populations of other EDisCS clusters with similar velocity dispersions and different redshifts.

Throughout this paper, we assume $H_0 = 70\,{\rm km\,s^{-1}\,Mpc^{-1}}$, $\Omega_{\rm m} = 0.30$, $\Omega_\Lambda = 0.70$. All magnitudes are in the Vega system.

2. The data

2.1. Target selection and observations

The target selection strategy, mask design procedure and observations are similar to those adopted for the EDisCS spectroscopy, described in detail in Halliday et al. (2004) and Milvang-Jensen et al. (2008). The only difference is that it targeted $z = 0.96$, unlike the previous target selection that was focused on $z = 0.70$.

The target selection was based on the available VLT/FORS2 optical photometry (White et al. 2005) and the NTT/SOFI NIR photometry (Aragón-Salamanca et al., in preparation). The optical data cover $6.5' \times 6.5'$ and are well-matched to the FORS2 spectrograph field-of-view. The NIR data cover a somewhat smaller region of $4.2' \times 5.4'$. The photometry was used as input to a modified version of the photometric redshifts code `hyperz` (Bolzonella et al. 2000). The aim of the target selection strategy was to keep all galaxies at the cluster redshift (brighter than $I = 23$), while removing objects that were almost certainly not galaxies at the cluster redshift. The selection criteria are explained in Halliday et al. (2004).

Targets already observed in previous runs and with measured redshifts (see Milvang-Jensen et al. 2008) were preferentially not repeated, when an alternative was found.

Poirier (2004) developed a programme to design the spectroscopic slit masks for EDisCS (called "MXU masks" after the Mask eXchange Unit in the FORS2 spectrograph). A fuller description of how the programme works is found in Halliday et al. (2004). Spectroscopic observations were completed using the FORS2 spectrograph[1] (cf. Appenzeller et al. 1998) on the VLT, during one observing run in March 2008, comprised of 3 half-nights. A high-efficiency grism was used (grism 600RI+19, $\lambda_{\rm central} = 6780$ Å, resolution FWHM ≈ 6 Å). The exposure time was 1800 seconds per frame, for a total of 8 frames per mask.[2] A total of 3 masks were observed, for a total of 94 slits (33 slits in mask 1 and 2 and 28 slits in mask 3).

2.2. Data reduction

The reduction was performed using an "improved sky subtraction", whose properties and advantages have been largely described and discussed in Milvang-Jensen et al. (2008). As presented in Milvang-Jensen (2003); Milvang-Jensen et al. (2003, 2008), the traditional sky subtraction did not work well for spectra produced by tilted slits: strong, systematic residuals were evident where skylines have been subtracted. As a consequence, an improved method for the sky subtraction was implemented. The method is described in detail in Kelson (2003). The key point of this method is that the sky subtraction is performed prior to any rebinning/interpolation of the data, hence it results in smaller noise than the traditional subtraction. Briefly, starting from the combined but uninterpolated frames, the data are flat-fielded; then the sky is fitted and subtracted and the spatial curvature is removed by means of an interpolation in y. The individual spectra are cut-out, the 2D wavelength calibration is applied by means of an interpolation in x, resulting in rectified 2D spectra (i.e. pixelised in $(x_{\rm r}, y_{\rm t})$) that are sky-subtracted, and with almost no systematic residuals where the skylines have been subtracted. Finally 1D spectra are extracted.

Around the central wavelength, our 1D spectra have a median S/N=4.6 Å per pixel in the continuum.

2.3. Galaxy redshifts and equivalent width determinations

Galaxy redshifts were measured from the reduced 1D spectra, using emission lines where possible, as done in Poggianti et al. (2006). We used the $[{\rm O\,II}]_{\lambda 3727}$ line, the $[{\rm O\,III}]_{\lambda 5007}$ line, the ${\rm H}\alpha_{\lambda 6563}$ line, or the most prominent absorption lines, e.g. Calcium K and H lines at 3934 Å and 3968 Å. The redshifts were manually assigned a quality flag. The vast majority of the measured redshifts (164/214) are of the highest quality, and these redshifts are assigned a 0 value in the $z_{quality}$ column in the catalogue. Secure redshifts but with larger uncertainties are assigned a $flag = 1$ (5/214), and doubtful redshifts are assigned a $flag = 2$ (9/214). For a fraction of objects (36/214), no redshift could be determined, and these redshifts are listed as 9.9999 in our data tables (flag $z_{quality} = 3$). The fraction of galaxies for which redshifts could not be obtained is somewhat higher than for the rest of the EDisCS clusters (Milvang-Jensen et al. 2008). This is due to the fact that this cluster is at significantly higher redshift and, although the magnitude limit in the target selection is the same, the target galaxies are, on average, significantly fainter than for the rest of EDisCS. In other words, the magnitude distribution is skewed towards fainter magnitudes, explaining the lower success rate. For the objects targeted as possible cluster members in the 3 long masks, the statistics are as follows: 10 stars, 204 galaxies and 36 without a determined redshift.

---

[1] `http://www.eso.org/instruments/fors`

[2] Only one frame of one mask had an exposure time of 2400 seconds.

In our sample, nine objects were already present in Milvang-Jensen et al. (2008). Two of them are stars (which were observed and repeated for calibration purposes), for one object the Milvang-Jensen et al. (2008) redshift estimate was more reliable. In the other cases, the difference between the two redshift estimates was always less than 0.0005. Milvang-Jensen et al. (2008), who adopted the same instruments, data reduction and procedure give an error that corresponds to ~ 0.0002, at any redshift, and this is compatible with the one computed as the difference between the two redshift estimates.

In addition, when possible, we also measured the equivalent width of [OII] and H_δ. Note that for star-forming galaxies the H_δ absorption line may be affected by emission in-filling. We have not attempted to correct for this effect.

From now on, we use both the spectra reduced in the current work and those already obtained by Milvang-Jensen et al. (2008) for the same field.

2.4. Spectroscopic completeness weights

During the EDisCS spectroscopic runs, slits were assigned to galaxies giving preference, whenever possible, to the brightest targets. Therefore, it is necessary to quantify how the completeness of the spectroscopic samples varies as a function of galaxy apparent magnitude. This was done comparing the number of objects in the spectroscopic catalogue with the number in the parent photometric catalogue in bins of I magnitude. The parent catalogue included all entries in the EDisCS photometric catalogue that were retained as targets for spectroscopy (see Halliday et al. 2004; Milvang-Jensen et al. 2008). Since here we compute spectroscopic completeness also for galaxies observed in Milvang-Jensen et al. (2008), we use as parent catalogue the sum of the parent catalogue used for the observations presented in Milvang-Jensen et al. (2008) plus the parent catalogue adopted for the current observations. The ratio of the number of objects in the spectroscopic catalogue to the number in the parent photometric catalogue yielded a weight as a function of galaxy apparent magnitude. The mean completeness for galaxies with $I < 23$ is $\sim 37\%$.

Geometrical effects, due to possible variations in the sampling as a function of the cluster-centric radius, can in principle affect a spectroscopic sample of a cluster. However, as discussed in Poggianti et al. (2006), geometrical effects are expected to be small when several masks of the same cluster, always centered on the cluster center, are taken, as it is the case for EDisCS. Hence we do not have to compute geometrical completeness weights.

2.5. Morphologies

The morphological classification of galaxies have been drawn from Desai et al. (2007) and it is based on the visual classication of HST/ACS F814W images sampling the rest-frame $\sim 4300-5500$ Å range. However, since 11/30 of our cluster and secondary structure members had no morphology in Desai et al. (2007), being fainter than the magnitude limit adopted in Desai et al. (2007), $ACS-HST$ images were inspected again[3] and a new morphology was assigned to the previously unclassified objects. It was very hard to assign a precise Hubble morphology for them. They are all peculiar, disturbed galaxies, possibly undergoing mergers.

The new morphological classification follows the one proposed by Desai et al. (2007). The classification is as follows: Star= 7, nonstellar but too compact to see structure= −6, ellipticals = −5, S0= 2, Sa= 1, Sb= 3, Sc= 5, Sd= 7, Sm= 9, Irr/Pec= 11, no HST data corresponding to ground-based object= 111.

2.6. Determining the galaxy stellar masses

In previous EDisCS papers (see, e.g, Vulcani et al. 2011), stellar masses were computed following the method proposed by Bell & de Jong (2001). However, the relation they proposed may not be valid at $z \sim 1$. This is because the spectro-photometric models they use are for $z \sim 0$, and assume that galaxies have been forming stars for the last $\sim 13\,Gyr$. In contrast, galaxies change their mass-to-light ratio over time, hence the assumptions that are valid at $z \sim 0$ might not be valid at high-z and the relation between mass-to-light ratio and colors could change going to higher redshifts. As a consequence, in this paper we determine stellar masses by fitting the observed photometry with a spectrophotometric model. We then compare the two approaches to test whether Bell & de Jong (2001) method is still valid at higher-z.

The model used in this paper follows the approach described in Hatziminaoglou et al. (2008, 2009) and was purposely modified to run with EDisCS data. It exploits the photometric EDisCS $VRIJK$ bands (White et al. 2005).

The aim of the GAlaxies SED FITting code (GASFIT) is to calculate the total stellar mass of galaxies from their observed photometry. The code uses a combination of theoretical spectra of Simple Stellar Population (SSP) models to reproduce the observed broad-band spectral energy distribution of a galaxy.

The Padova evolutionary tracks (Bertelli et al. 1994) and a standard Salpeter (1955) IMF, with masses in the range $0.15-120\,M_\odot$ are used. For details on the set of SSP see Fritz et al. (2007, 2011) and references therein. The final set of SSPs is composed of 13 spectra referring to stellar ages ranging from 3×10^6 to 14×10^9 years. The set has a common metallicity which can be chosen by the user. All the spectra are weighted with a suitable value of the stellar mass, then they are summed. The effect of dust attenuation is taken into account by applying an extinction law, which is simulating dust distributed in a uniform slab sitting in front of the stars; a common value is adopted for all SSPs, i.e. no selective extinction is considered. The Galactic extinction curve is generally adopted, but the code allows for other options as well. The amount of extinction, which is measured through the $E(B-V)$ value, is one of the parameters of the code.

The value of the stellar mass that is used to weight the spectra of each age, is computed by assuming that the star formation history (SFH), that is the star formation rate as a function of time, of a galaxy is well represented by a "delayed–exponential" law (Sandage 1986; Gavazzi et al. 2002).

---

[3] This has been done by three independent classifiers, Benedetta Vulcani, Bianca M. Poggianti and Alfonso Aragón-Salamanca.

The final model spectrum is hence computed. Once the metallicity of the stars and the extinction law are fixed, only two free parameters are used: $E(B-V)$ and τ, which is expressed in terms of the age of the galaxy. To find the combination of these two parameters that minimizes the difference between the observed photometry and the model, models are calculated for various combinations of $E(B-V)$ and τ, where the first parameter can assume values ranging from 0 to 0.2[4] and the second can range from 0.02 to 1. The best-fit model is chosen as the one yielding the lowest χ^2 value. This procedure is repeated for each object of the input catalogue. The total stellar mass values provided by the code include the mass in stars plus stellar remnants.

Stellar masses have been computed for all galaxies with a reliable redshift. Since the model adopts a Salpeter (1955) IMF in the mass range $0.15-120\,M_{\odot}$, to convert to a Kroupa (2001) IMF we multiplied the model masses by a factor $1/1.33$. Given the mass range of the galaxy sample, we used models with solar metallicity.

We compare the results coming from these models to the masses computed using Bell & de Jong (2001) for cluster members and found that both methods give compatible mass estimates (rms ~ 0.1 dex), suggesting that the Bell & de Jong (2001) relation and detailed SED-fitting methods give similar results even at $z \sim 0.95$.

To compute the mass completeness limit we consider the main structure, at $z \sim 0.96$, and determine the value of the mass of a galaxy with an absolute B magnitude corresponding to $I = 23$, and a color $(B-V) \sim 0.85$, which is the reddest color of galaxies in this cluster. In this way, the limit for a Kroupa (2001) IMF is $M_* \geq 10^{10.7} M_{\odot}$.

2.7. The spectroscopic catalogue

All the previously-available EDisCS spectroscopic information is described in Halliday et al. (2004) and Milvang-Jensen et al. (2008). The catalogue presented here contains all the spectroscopy now available for this cluster field, including our new data and the data presented in Milvang-Jensen et al. (2008) for completeness.

The format of the tables is illustrated in Table 1, while the whole catalogue is published electronically at the CDS.

Column 1 gives the object name *ID*. (IDs starting with EDCS**N**J), usually adopted to indicate EDisCS galaxies. These IDs are derived from the EDisCS photometric catalogue, matching the coordinates (RA and DEC).

Column 2 gives $I_{\rm auto}$, the total I-band magnitude (not corrected for Galactic extinction). This magnitude comes from the catalogues published in White et al. (2005).

Column 3 gives the redshift z as determined in §2.3. The redshifts are always given with 4 decimal places. A value of 0.0000 denotes a star, and 9.9999 denotes that no redshift could be determined.

Column 4 gives the redshift quality $z_{\rm quality}$. 0 means that redshift measurement is robust. Secure redshifts but with larger uncertainties are assigned a flag=1, doubtful redshifts are assigned a flag=2, no redshift estimates are assigned a flag=3.

Column 5 gives the membership flag. It is 1 for members of the main cluster, 1c, 1d, 1e for members of secondary structures, 0 for field galaxies, and "–" for stars and objects without a determined redshift. Membership is defined as being within $\pm 3\ \sigma_{\rm cl}$ from $z_{\rm cl}$.

Column 6 gives $EW_{\rm OII}$, the rest-frame equivalent width, in Å, of the $[\mathrm{O\,II}]_{\lambda 3727}$ line, adopting the convention that EWs are negative when in emission. "–" indicates the measurement was not possible due to low S/N.

Column 7 gives $EW_{\rm H_\delta}$, the rest-frame equivalent width, in Å, of the H_δ line, adopting the convention that EWs are negative when in emission. "–" indicates the measurement was not possible due to low S/N.

Column 8 gives the mass estimates, computed as presented in §2.6 and converted to a Kroupa (2001) IMF.

Column 9 gives the spectroscopic magnitude completeness weights, computed as presented in §2.4.

Column 10 gives the morphology of galaxies.

Column 11 gives some relevant comments.

3. Results

3.1. Galaxy positions, redshifts and cluster velocity dispersions

In this section, we study the distribution of galaxies in the field, investigating whether they are grouped in structures. We study both their spatial and redshift distributions.

The lower right panel of Figure 1 shows the redshift histogram obtained from the spectroscopic observations of the field. Here all galaxies are used, both those for which we carried out the data reduction and those already analyzed by Milvang-Jensen et al. (2008). In the redshift distribution four structures can be detected, called 1 (the main peak at the cluster redshift), 1c, 1d and 1e, characterized in Table 2.

Table 2. List of the structures identified, with redshift, and number of members.

name	z	$N_{\rm memb}$
1 (cluster)	0.958	22 (22)
1d	0.825	8 (6)
1c (secondary structure)	0.983	7 (6)
1e	0.807	4 (2)

Notes – The number of members is within $\pm 3\sigma$ from the structure's redshift. In parenthesis the number of objects with a reliable redshift ($z_{\rm quality} = 0$) is given. The structures are labelled in richness order, with the richest (as determined from the number of spectroscopic members) first.

The upper right panel of the Figure 1 shows a zoom of the redshift histograms of the structures 1 and 1c that will be analyzed carefully in the following. The other structures, 1d and 1e, will be discarded from our galaxy analysis since they are outside the targeted redshift range and the galaxies observed are therefore a biassed subsample of the total population.

To compute velocity dispersions we adopt the iterative method used in Milvang-Jensen et al. (2008), using a biweight scale estimator (Beers et al. 1990). The rest-frame velocity dispersion obtained for the main structure is quite robust and reliable: $\sigma_{\rm rf} = 522^{+111}_{-111}\,{\rm km\,s^{-1}}$. However, we note that although in this work 13 spectra were added, the error in sigma did not appreciably decrease from the value found in Milvang-Jensen et al. (2008) (see §3.2.1), which implies that the structure is not relaxed. The velocity dispersions for all other structures are very uncertain, hence not useful for the following analysis. In Table 3 additional information for the Cl 1103.7−1245 cluster is given.

---

[4] We note that even extending the E(B-V) range up to 1 the results do not change significantly.

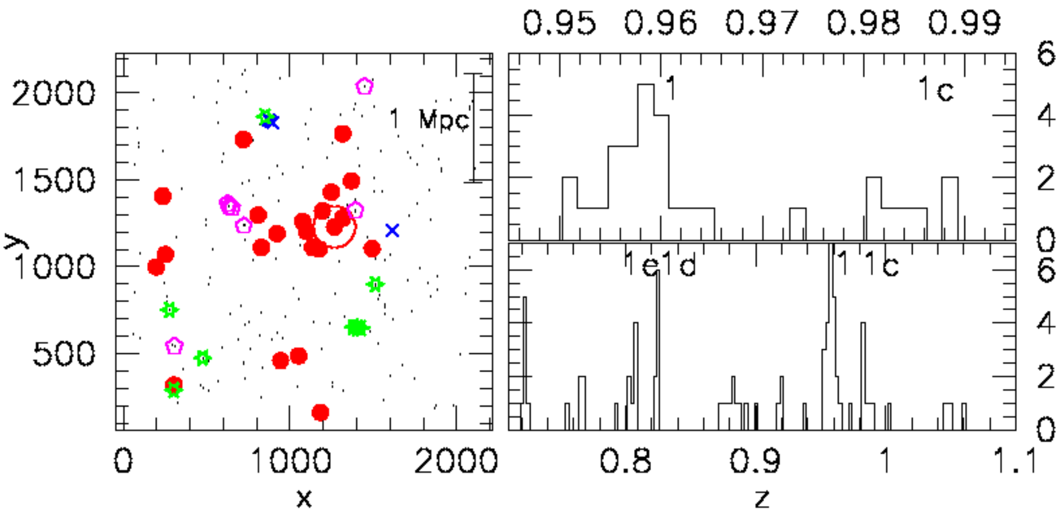

Fig. 1. Left panel: spatial distribution of galaxies in the whole field. Pixel positions for galaxies are given. The units on the axes are pixels = 0.2″. North is up and east is to the left .The structures identified are indicated with the different colors. Black points: all galaxies in the spectroscopic catalog. Red dots: main cluster, "1". Empty magenta pentagons: "1c". Green skeletal stars: "1d". Blue crosses: "1e". The size of 1 Mpc at $z = 0.95$ is also shown. The BCG of the main cluster is also indicated with an empty red circle. Lower right panel: redshift histogram of the whole field. The position of the structures identified in the field is also indicated. Upper right panel: redshift histogram of the structures 1 and 1c, which are the structures analyzed in the paper.

For the sake of completeness, we mention that we obtained $\sigma_{\rm rf} = 517^{+204}_{-124}$km s^{-1} for the secondary structure 1c, $\sigma_{\rm rf} = 167^{+65}_{-34}$km s^{-1} for structure 1d, and $\sigma_{\rm rf} = 34^{+18}_{-18}$km s^{-1} for structure 1e, although we insist these are highly unreliable.

The left panel of Figure 1 shows the spatial distribution of galaxies in the entire field. The structures identified are indicated with the different colors. Most of the galaxies of the main structure are concentrated around the BCG (see below), while galaxies of the other structures are very spread and it is not possible to define the position of the center.

It is interesting to note that, even though the secondary structure has a very similar velocity dispersion value as the main cluster, it has ×3 fewer members. It is also close to the main structure both in redshift and in physical distance (their distance is $\sim 13\sigma$). This probably indicates that the secondary structure is not quite a cluster yet, but some smaller system possibly infalling onto the main cluster at later time.

Due to the small number of members, we are not able to identify any substructure in any of the structures.

In this section, we have investigated the structures found in the field, we can now proceed characterizing in detail the galaxy populations of two of them: the structures 1 and 1c.

3.2. Analysis of the galaxy properties and stellar populations

3.2.1. The Cl 1103.7−1245 cluster

In this subsection we carefully analyze the properties of Cl 1103.7−1245, the main structure identified in the field. Our spectroscopic catalogue of this cluster now consists of 22 galaxies. When Milvang-Jensen et al. (2008) observed it, they found only 9 members with robust redshift measurements. They measured $z_{cl} = 0.9586$ and $\sigma_{cl} = 534^{+101}_{-120}$ km s^{-1}. Putting all data together, we find $z_{cl} = 0.9580$ and $\sigma_{cl} = 522 \pm 111$ km s^{-1}.

One of our new members was also tentatively assigned as cluster member by the ERGS project (Douglas et al. 2010), using a lower resolution grism.

Other pieces of information for this field can be found in White et al. (2005) and Pelló et al. (2009). Using all of these, we characterize the galaxy population of both the cluster and the secondary structure (see §3.2.2).

For one galaxy member, EDCSNJ1103464−1248034, the photometry was not reliable, due to the presence of a galaxy close to it that altered its observed photometry, hence values of magnitudes, colors, and mass are not reliable. It will be disregarded in the following analysis.

White et al. (2005) gave the position of the BCG candidate for each EDisCS cluster. As already found by the previous EDisCS data, the galaxy proposed to be the BCG for this cluster actually is the most luminous cluster member galaxy. This galaxy is EDCSNJ1103434−1245341 and its position is shown in the left panel of Figure 1. It appears that the BCG lies towards the edge of the distribution of members, arguing that this cluster is not relaxed and that there may be a significant systematic error in the velocity dispersion. Another explanation to the fact that there are no objects on the right hand side of the field could be that that region has been observed during the old run, which was unfavorable to z=0.96, hence it was hard to find cluster members.

In Figure 2 the color magnitude diagram for cluster members (filled symbols) and secondary structure members (empty symbols) is shown. Morphological types and measured values of the EW([O ii]) are also indicated, with different colors and symbols. Rest-frame absolute B magnitude and rest-frame $(B-V)_0$ are derived from photo-z fitting, fixing each galaxy redshift to be equal to the spectroscopic redshift of the cluster (Rudnick et al. 2003; Pelló et al. 2009).

Among the spectroscopic members, three galaxies are ellipticals, eleven are spirals, seven are irregulars/peculiars and one is located outside the ACS image. It is interesting to note that no S0 galaxies are detected. All ellipticals have red colors, are located on the red sequence and do not have any significant star formation ([O ii] was detected only in one elliptical galaxy with a very low EW, probably due to AGN activity). These are the brightest and the most massive galaxies (see below for the mass distribu-

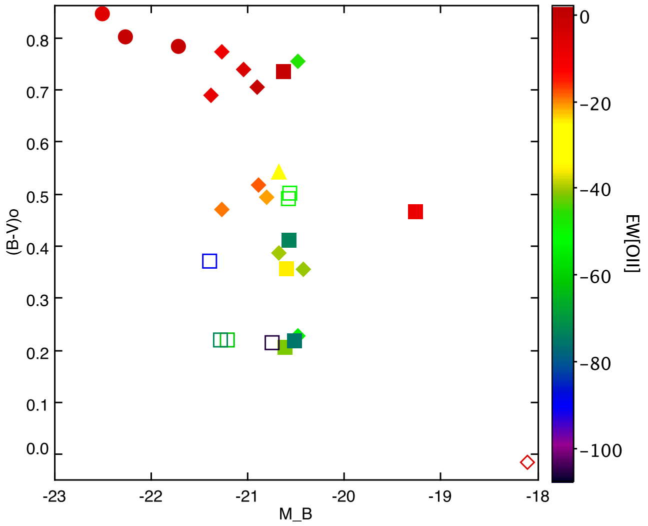

Fig. 2. Rest-frame $(B - V)_0$ vs. M_B diagram for spectroscopic members of the cluster 1 (filled symbols) and the secondary structure 1c (empty symbols), with also the morphology and the [OII] (color coded) information. Circles: ellipticals. Diamonds: spirals. Squares: irregulars/peculiars. Triangles: galaxy out of the ACS image.

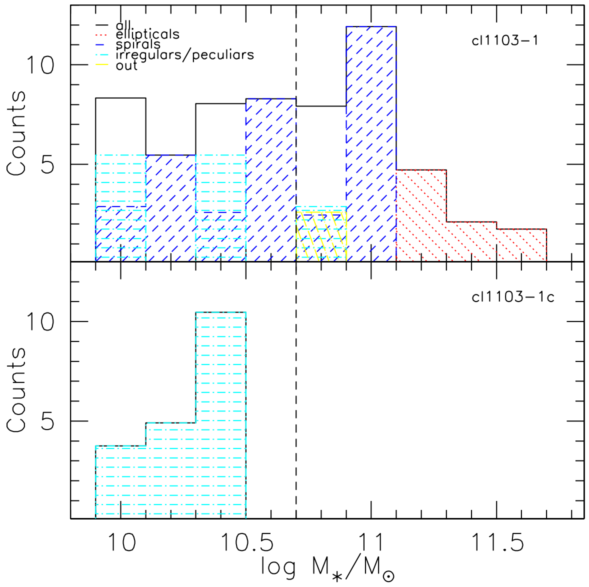

Fig. 3. Weighted mass distribution of galaxies in the cluster. All (black line), elliptical (red line), spiral (blue line), and irregular/peculiar (cyan line) galaxies are shown. Also the galaxy without morphology is indicated (yellow line). The mass completeness limit is indicated with a dashed vertical line. Upper panel: cluster 1, lower panel: secondary structure 1c.

tion). The BCG of the cluster is an elliptical galaxy. In contrast, late-type galaxies (spirals + irregulars/peculiars), which represent the vast majority of the entire sample, cover a wide color range. Six of them have quite red colors and are located on the red sequence. This may be due to the presence of dust. In fact, as proposed by Wolf et al. (2009), optically-passive spirals in clusters, and dusty red galaxies appear to be basically the same phenomenon. These objects are not truly passive galaxies despite their red colors. The other late-types belong to the blue cloud. All late-type galaxies show [OII] emission lines in their spectrum, hence they are assumed to be star-forming. On the whole, the [OII] in emission has been measured for 17/22 galaxies. All galaxies with no [OII] or with very weak emission lines are located on the red sequence.

In the upper panel of Figure 3 the mass distribution of cluster galaxies weighted for spectroscopic incompleteness is shown. Galaxies cover a quite wide range of masses ($9.9 \leq \log M_*/M_\odot \leq 11.8$). The mass distributions of galaxies of different morphological types are also indicated. Ellipticals and late-types follow two distinct mass distributions. All ellipticals have $\log M_*/M_\odot \geq 11.1$, while late-types have $\log M_*/M_\odot \leq 11.1$.

Our sample is complete in mass for all galaxy types down to $\log M_*/M_\odot \sim 10.7$, and the differences in mass distribution between ellipticals and late-types are clearly noticeable above this limit.

3.2.2. The secondary structure Cl 1103.7-1245c

In this subsection we study the galaxy population of Cl 1103.7-1245c, called secondary structure, which is represented by empty magenta pentagons in the left panel of Figure 1. Our sample in this structure consists of seven galaxies. It is a diffuse structure and, except for three galaxies that are close both in space and in redshift, members are far from each other. Due to the small number of galaxy members, the color magnitude diagram is sparsely populated (see empty symbols in Fig. 2). The red sequence can not be detected; all galaxies are placed in the blue cloud.

One galaxy is located outside the ACS image and hence has no known morphology. All others are irregulars/peculiars. Moreover, all galaxies in this structure have strong emission lines and are therefore strongly star forming.

Comparing the results for the cluster and the secondary structure, we find that they consist of very different galaxy populations. The cluster hosts both a population of passive galaxies and at least one star-forming one, while in the secondary structure all galaxies are star-forming. Also the mass distributions are different: galaxies have systematically lower masses in the secondary structure than in the cluster.

To investigate whether the galaxy mass might be the main driver of the detected differences in the cluster and the secondary structure we consider only cluster galaxies in the mass range of secondary structure galaxies ($9.9 \leq M_*/M_\odot \leq 10.5$). These galaxies are all late-types and all of them are star-forming ([OII] detected). Four of them are spirals, four are irregulars/peculiars. In contrast, all secondary structure galaxies are irregulars and star forming. Thus, even if we consider only a common mass range, the galaxy population in cluster 1 and in structure 1c seem to be different, with less evolved galaxies in the latter.

Even though our sample is affected by low number statistic, it is worth noting that, neither in the cluster nor in the secondary structure do we detect galaxies in a transient phase, such as those moving from the blue cloud to the red sequence, or post-starburst galaxies (objects characterized by strong Balmer lines in absorption and no emission lines, indicating that the star formation activity ended abruptly during the past ~Gyr). We note that the lack of E+A galaxies is consistent with the number expected from lower redshift EDisCS clusters.

3.3. Comparisons with lower redshift clusters

The analysis presented in this paper allows us to significantly extend the redshift range of the EDisCS survey. It is therefore interesting to compare the galaxy population of Cl 1103.7−1245 with those in other EDisCS clusters to detect possible evolutionary trends. For comparison we select all the EDisCS structures that have a similar velocity dispersion but are located at lower redshifts. Table 4 lists the clusters that satisfy these requirements.

We first adopt a common absolute magnitude limit (corrected for passive evolution[5]). For Cl 1103.7−1245, the completeness magnitude limit is fixed at $M_V = -21$. Hence, for the other clusters we adopt a limit which for passively-evolving galaxies corresponds to $M_V = -21$ at $z \sim 0.95$ (see Table 4). At any redshift, we consider only galaxies within $0.8R_{200}$. This corresponds to the spectroscopic coverage of the clusters at $z \sim 0.4$.

In this section we compare the completeness-corrected number of cluster members, the completeness-weighted fraction of galaxies with [OII] in emission, and, when available, the completeness-weighted morphological fractions. In Table 4 numbers and fractions for each cluster are given.

In Figure 4 the completeness-corrected number of members of each cluster is plotted as a function of z. The number of galaxy members in clusters with similar velocity dispersion seems to decrease with redshift. The only exception in this trend is for Cl 1054.7-1245 that has many more members. This can be due to the presence of a secondary structure close to the main cluster that is difficult to disentangle.

As found in Poggianti et al. (2010) in simulations, the number of cluster members per unit of cluster mass is constant both with redshift and cluster mass ($N_{\rm memb} = \alpha M_{\rm sys}$). These authors computed $\alpha = 20\,{\rm galaxies}/10^{14}\,M_\odot$ for a magnitude limit $M_V = -20$. At $z = 0.45$, for a cluster $\sigma = 500\,{\rm km\,s^{-1}}$, we estimate the cluster halo mass to be $M_{\rm sys} = 1.686 \times 10^{14}\,M_\odot$.[6] Considering Cl 1202.7−1224 and Cl 1018.8−1211 (whose mean redshift is $\langle z \rangle = 0.45$ and mean velocity dispersion is $\langle \sigma \rangle \sim 500\,{\rm km\,s^{-1}}$), we measure a number of members equal to 43 for our magnitude limit of $M_V = -20.5$. Therefore $\alpha = 25.5\,{\rm galaxies}/10^{14}\,M_\odot$. As a consequence, the predicted number of galaxies for a cluster of the same velocity dispersion, but located at $z = 0.95$ is ~ 32 (this calculation reflects the growth of the halo mass with cosmic time). This is in good agreement with the observations shown in Figure 4: Cl 1103.7−1245 has 31.4 galaxies and a velocity dispersion of $522 \pm 111\,{\rm km\,s^{-1}}$.

We now explore the evolution of the star-formation activity of the galaxies in these clusters using the [OII] emission line as a tracer. Looking at the fraction of galaxies with [OII] emission (see Table 4),[7] a slight trend with z is detected: Cl 1103.7−1245 has a marginally higher fraction of star-forming galaxies than lower-z clusters.

Concerning galaxy morphologies (see Table 5), Cl 1103.7−1245 seems to follow the trends found in Desai et al. (2007): there is no significant redshift evolution in the elliptical galaxy fraction, but there is a clear decline in the S0 fraction with look-back-time. Indeed, none of the spectroscopic members of Cl 1103.7−1245 is an S0, while we find a relatively-high fraction of late-type galaxies. However, the absence of S0s could simply be due to the small sample size: at these redshifts the fraction of S0s found in clusters is quite small (Postman et al. 2005).

To compare galaxy stellar masses between clusters we adopt mass-limited samples with $\log M_*/M_\odot \geq 10.7$, which are complete at all redshifts. The mean stellar masses of cluster galaxies are very similar for all the clusters (Table 4). This suggests that the high-mass end of the galaxy population in clusters of similar velocity dispersion has not changed much in the redshift range explored, i.e., the most massive galaxies were already in place in $z \sim 1$ clusters.

4. Summary

In this paper we present new spectroscopic observations for Cl 1103.7−1245, the most distant cluster of the EDisCS project ($z = 0.9580$), complementing the previous analysis of Milvang-Jensen et al. (2008), whose observations targetted z=0.70 and thus were somewhat biased against galaxies in this cluster at z=0.96

From the spectra we measured the galaxies' redshifts, $[{\rm O\,II}]_{\lambda 3727}$ and H_δ equivalent widths, and spectroscopic completeness weights. These new data were complemented with information from White et al. (2005) and Pelló et al. (2009), to characterise the galaxies' physical properties such as their stellar masses, star-formation activities and morphologies. This allowed us to study the galaxy populations in the Cl 1103.7−1245 cluster ($z = 0.9580$) and another structure at a similar redshift (Cl 1103.7−1245c at $z = 0.9830$), and compared them with those of lower redshift clusters. The main results can be summarised as follows:

- The main cluster Cl 1103.7−1245 (for which we have 22 spectroscopic members) consists of two well separated populations: elliptical galaxies located on the red sequence without any significant star-formation activity, and active late-type galaxies, that can be either as red as the red sequence galaxies or cover a wide range of colors. All morphologically late-type galaxies are star-forming. The cluster galaxies cover quite a broad range of masses ($9.9 \leq \log M_*/M_\odot \leq 11.8$). All ellipticals are very massive ($\log M_*/M_\odot \geq 11.1$), while the late-types (spirals and irregulars) have $\log M_*/M_\odot \leq 11.1$.

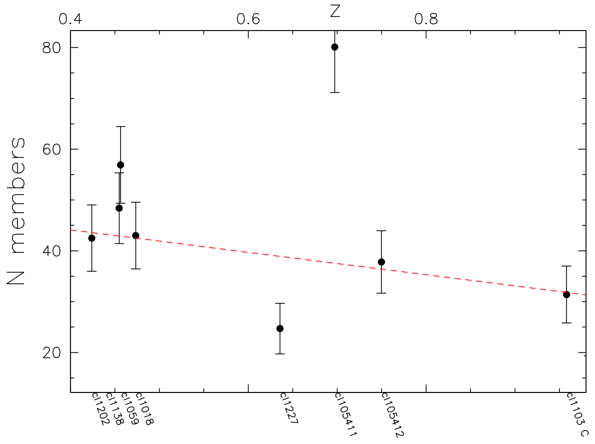

Fig. 4. Completeness-corrected number of cluster members as a function of redshift for EDisCS clusters with $\sigma = 500\,{\rm km\,s^{-1}}$. The predicted number of cluster members for the adopted magnitude limit is shown as the red dashed line. See text for details.

---

[5] The passive evolution has been computed assuming the formation at z=5 and solar metallicity.

[6] We compute the mass of the system as in Poggianti et al. (2006).

[7] In computing the [OII] fractions, we consider only galaxies for which the [OII] line could be measured (even if absent). However, in each cluster at most 1 or 2 galaxies had no EW([OII]) measurement.

– Cl 1103.7-1245c, the secondary structure, (for which we have 7 spectroscopic members) contains only irregular/peculiar galaxies, with some possibly undergoing mergers. These galaxies are all star forming and located in the blue cloud. Their stellar masses are in the $9.9 \leq \log M_*/M_\odot \leq 10.5$ range, systematically less massive than the galaxies in the main cluster.

We conclude that the main cluster and the secondary structure consist of very different galaxy populations, with clearly different star formation properties, morphologies and masses.

We have also compared the properties of the Cl 1103.7−1245 cluster galaxies with those of the galaxy populations in EDisCS clusters at lower redshift and comparable velocity dispersions ($\sigma_{\rm clus} \simeq 500\,{\rm km\,s^{-1}}$). Considering absolute-magnitude-limited samples ($M_V \leq -21$ at $z \sim 0.95$), and galaxies within $0.8R_{200}$, the main results are:

– The number of member galaxies in clusters with similar velocity dispersions decreases slightly with redshift. This is a consequence of the fact that the cluster mass is expected to grow with time and the prediction from simulations that the number of galaxies per unit of cluster mass should be independent of redshift and cluster halo mass (Poggianti et al. 2010).

– The morphologcal mix and the star-formation activity in the cluster galaxies follows the trends found at lower redshifts. The fraction of elliptical galaxies remains approximately constant with redshift, while the fraction of S0s declines as the fraction of later types increases. We found no spectroscopically-confirmed S0s in Cl 1103.7−1245. Furthermore, the fraction of star-forming galaxies in this cluster is marginally higher than in lower-redshift clusters of similar $\sigma_{\rm clus}$.

Finally, comparing mass-limited galaxy samples with $\log M_*/M_\odot \leq 10.7$, we found that the galaxies in clusters of similar $\sigma_{\rm clus}$ have similar average stellar masses, suggesting that the most massive galaxies were already in place in at $z \sim 1$ clusters.

Acknowledgements. We thank the referee for her/his useful comments which helped us to improve our manuscript. BV and BMP acknowledge financial support from ASI contract I/016/07/0 and ASI-INAF I/009/10/0. BV also acknowledges financial support from the Fondazione Ing. Aldo Gini and thanks the School of Physics and Astronomy, Univeristy of Nottingham, for a very pleasant and productive stay during which part of the work presented in this paper was carried out. The Dark Cosmology center is funded by the Danish National Research Foundation. BMJ acknowledges support from the ERC-StG grant EGGS-278202.

References

Appenzeller, I., Fricke, K., Fürtig, W., et al. 1998, The Messenger, 94, 1
Aragon-Salamanca, A., Ellis, R. S., Couch, W. J., & Carter, D. 1993, MNRAS, 262, 764
Balogh, M. L., Morris, S. L., Yee, H. K. C., Carlberg, R. G., & Ellingson, E. 1997, ApJ, 488, L75
Bamford, S. P., Milvang-Jensen, B., Aragón-Salamanca, A., & Simard, L. 2005, MNRAS, 361, 109
Beers, T. C., Flynn, K., & Gebhardt, K. 1990, AJ, 100, 32
Bell, E. F. & de Jong, R. S. 2001, ApJ, 550, 212
Bertelli, G., Bressan, A., Chiosi, C., Fagotto, F., & Nasi, E. 1994, A&AS, 106, 275
Bolzonella, M., Miralles, J.-M., & Pelló, R. 2000, A&A, 363, 476
Clowe, D., Schneider, P., Aragón-Salamanca, A., et al. 2006, A&A, 451, 395
Couch, W. J. & Sharples, R. M. 1987, MNRAS, 229, 423
Demarco, R., Rosati, P., Lidman, C., et al. 2007, ApJ, 663, 164
Desai, V., Dalcanton, J. J., Aragón-Salamanca, A., et al. 2007, ApJ, 660, 1151
Douglas, L. S., Bremer, M. N., Lehnert, M. D., Stanway, E. R., & Milvang-Jensen, B. 2010, MNRAS, 409, 1155
Dressler, A., Smail, I., Poggianti, B. M., et al. 1999, ApJS, 122, 51
Fassbender, R., Böhringer, H., Santos, J. S., et al. 2011, A&A, 527, A78
Finn, R. A., Zaritsky, D., McCarthy, Jr., D. W., et al. 2005, ApJ, 630, 206
Fritz, J., Poggianti, B. M., Bettoni, D., et al. 2007, A&A, 470, 137
Fritz, J., Poggianti, B. M., Cava, A., et al. 2011, A&A, 526, A45+
Gavazzi, G., Bonfanti, C., Sanvito, G., Boselli, A., & Scodeggio, M. 2002, ApJ, 576, 135
Gilbank, D. G., Yee, H. K. C., Ellingson, E., et al. 2007, AJ, 134, 282
Gonzalez, A. H., Zaritsky, D., Dalcanton, J. J., & Nelson, A. 2001, ApJS, 137, 117
Halliday, C., Milvang-Jensen, B., Poirier, S., et al. 2004, A&A, 427, 397
Hatziminaoglou, E., Fritz, J., Franceschini, A., et al. 2008, MNRAS, 386, 1252
Hatziminaoglou, E., Fritz, J., & Jarrett, T. H. 2009, MNRAS, 399, 1206
Jørgensen, I., Bergmann, M., Davies, R., et al. 2005, AJ, 129, 1249
Jørgensen, I., Chiboucas, K., Flint, K., et al. 2006, ApJ, 639, L9
Kelson, D. D. 2003, PASP, 115, 688
Kelson, D. D., Illingworth, G. D., Franx, M., & van Dokkum, P. G. 2006, ApJ, 653, 159
Kelson, D. D., van Dokkum, P. G., Franx, M., Illingworth, G. D., & Fabricant, D. 1997, ApJ, 478, L13
Kroupa, P. 2001, MNRAS, 322, 231
Levine, E. S., Schulz, A. E., & White, M. 2002, ApJ, 577, 569
Lima, M. & Hu, W. 2004, Phys. Rev. D, 70, 043504
Milvang-Jensen, B. 2003, PhD thesis, University of Nottingham, NG7 2RD Nottingham, UK
Milvang-Jensen, B., Aragón-Salamanca, A., Hau, G. K. T., Jørgensen, I., & Hjorth, J. 2003, MNRAS, 339, L1
Milvang-Jensen, B., Noll, S., Halliday, C., et al. 2008, A&A, 482, 419
Moran, S. M., Ellis, R. S., Treu, T., et al. 2005, ApJ, 634, 977
Muzzin, A., Wilson, G., Yee, H. K. C., et al. 2012, ApJ, 746, 188
Olsen, L. F., Zucca, E., Bardelli, S., et al. 2005, A&A, 442, 841
Pelló, R., Rudnick, G., De Lucia, G., et al. 2009, A&A, 508, 1173
Poggianti, B. M., De Lucia, G., Varela, J., et al. 2010, MNRAS, 405, 995
Poggianti, B. M., Smail, I., Dressler, A., et al. 1999, ApJ, 518, 576
Poggianti, B. M., von der Linden, A., De Lucia, G., et al. 2006, ApJ, 642, 188
Poirier, S. 2004, PhD thesis, Louis Pasteur University, Strasbourg I, France
Postman, M., Franx, M., Cross, N. J. G., et al. 2005, ApJ, 623, 721
Postman, M., Lubin, L. M., & Oke, J. B. 1998, AJ, 116, 560
Postman, M., Lubin, L. M., & Oke, J. B. 2001, AJ, 122, 1125
Rudnick, G., Rix, H.-W., Franx, M., et al. 2003, ApJ, 599, 847
Salpeter, E. E. 1955, ApJ, 121, 161
Sandage, A. 1986, ARA&A, 24, 421
Serote Roos, M., Lobo, C., Durret, F., Iovino, A., & Márquez, I. 2005, A&A, 429, 101
Tanaka, M., Kodama, T., Arimoto, N., & Tanaka, I. 2006, MNRAS, 365, 1392
Tran, K.-V. H., Franx, M., Illingworth, G., Kelson, D. D., & van Dokkum, P. 2003, ApJ, 599, 865
Tran, K.-V. H., Franx, M., Illingworth, G. D., et al. 2007, ApJ, 661, 750
van Dokkum, P. G., Franx, M., Fabricant, D., Illingworth, G. D., & Kelson, D. D. 2000, ApJ, 541, 95
Vulcani, B., Poggianti, B. M., Aragón-Salamanca, A., et al. 2011, MNRAS, 412, 246
White, S. D. M., Clowe, D. I., Simard, L., et al. 2005, A&A, 444, 365
Wolf, C., Aragón-Salamanca, A., Balogh, M., et al. 2009, MNRAS, 393, 1302
Yee, H. K. C., Ellingson, E., & Carlberg, R. G. 1996, ApJS, 102, 269

Table 1. Illustration of the format of the spectroscopic catalogues.

ID new	$I_{\rm auto}$	z	$z_{\rm qual}$	memb	$EW_{\rm OII}$	$EW_{\rm H_\delta}$	$\log M_*/M_\odot$	W	morph	comm
...	...	...	...	...	...	...	...	...	...	
EDCSNJ1103444−1245153	21.534	0.9640	0	1	0.0	2.5	11.243	4.71	−5	...
EDCSNJ1103447−1245597	22.213	0.9588	0	1	−20.8	4.0	10.404	2.58	3	...
EDCSNJ1103417−1245150	22.188	0.9885	0	1c	−105.5	−8.0	10.087	3.75	11	...
EDCSNJ1103437−1244540	22.168	0.9559	0	1	−17.8	—	10.538	3.75	5	...
EDCSNJ1103462−1245556	22.289	0.7212	0	0	−66.95	—	9.748	2.58	1	...
...	...	...	...	...	...	...	...	...	...	

Notes – This example table contains entries to illustrate all relevant features of the tables published electronically at the CDS. This table contains both the new redshifts from data presented in this work (56% of the redshifts) and all the redshifts taken in this field from the previous EDisCS spectroscopy (Milvang-Jensen et al. 2008) (44% of the redshifts).

Table 3. R_{200}, M_σ, and M_{lens} for Cl 1103.7−1245.

name	$\sigma_{\rm rf}$ (km s^{-1})	R_{200} (Mpc)	M_σ ($M_\odot$)	M_{lens} ($M_\odot$)
Cl 1103.7−1245	522^{+111}_{-111}	0.76 ± 0.16	$(1.42 \pm 0.99) \times 10^{14}$	$(7.25 \pm 3.48) \times 10^{14}$

Notes – The virial radius R_{200}, defined as the radius delimiting a sphere with interior mean density 200 times the critical density of the Universe at that redshift, was computed as in Poggianti et al. (2006), the masses M_σ was computed following Finn et al. (2005), and M_{lens} is from Clowe et al. (2006). Errrors were computed with the propagation of errors.

Table 4. EDisCS clusters used to compare galaxy populations. Number of members, magnitude limit and [OII] fractions for all clusters.

name	z	σ (km s^{-1})	N	M_V	f([OII])	$\langle\log(M_*/M_\odot)\rangle^1$
Cl 1202.7−1224	0.4240	518^{+92}_{-104}	42.5	−20.5	0.27 ± 0.08	10.97 ± 0.04
Cl 1138.2−1133a	0.4548	542^{+63}_{-71}	48.8	−20.5	0.64 ± 0.08	10.9 ± 0.05
Cl 1059.2−1253	0.4564	510^{+52}_{-56}	56.9	−20.5	0.62 ± 0.07	11.08 ± 0.02
Cl 1018.8−1211	0.4734	486^{+59}_{-63}	43.0	−20.6	0.37 ± 0.09	10.97 ± 0.04
Cl 1227.9−1138	0.6357	574^{+72}_{-75}	24.7	−20.7	0.63 ± 0.01	11.02 ± 0.06
Cl 1054.4−1146	0.6972	589^{+78}_{-70}	80.1	−20.8	0.62 ± 0.06	11.08 ± 0.04
Cl 1054.7−1245	0.7498	504^{+113}_{-65}	37.8	−20.8	0.18 ± 0.08	11.19 ± 0.02
Cl 1103.7−1245	0.9580	522^{+111}_{-111}	31.4	−21.0	0.76 ± 0.12	11.06 ± 0.03

^{1}Mean masses are computed above the common mass limit $\log(M_*/M_\odot) \geq 10.7$.

Table 5. Morphological fractions (in %) for all clusters, above the absolute magnitude limit $M_V \leq -21$ at $z = 0.95$, corrected for passive evolution.

name	compacts	ellipticals	S0s	spirals	irr/pec
Cl 1138.2−1133a	0±2	27±7	11±6	62±8	0±2
Cl 1227.9−1138	0±4	13±8	30±12	58±13	0±4
Cl 1054.4−1146	6±3	32±6	0±1	53±6	9±4
Cl 1054.7−1245	0±2	43±5	24±4	33±5	0±2
Cl 1103.7−1245	0±3	27±9	0±3	73±9	0±3